PNAS RESEARCH ARTICLE | IMMUNOLOGY AND INFLAMMATION

The epithelial *C15ORF48/miR-147-NDUFA4* axis is an essential regulator of gut inflammation, energy metabolism, and the microbiome

Min Xiong[a], Ze Liu[b], Bintao Wang[a], Thomas Sokolich[a], Natalie Graham[a], Meirong Chen[c], Wei-Le Wang[a], and Mark P. Boldin[a,1]

Affiliations are included on p. 11.

Edited by Marco Colonna, Washington University in St. Louis School of Medicine, St. Louis, MO; received September 19, 2023; accepted May 13, 2024

Chronic inflammation is epidemiologically linked to the pathogenesis of gastrointestinal diseases, including inflammatory bowel disease (IBD) and colorectal cancer (CRC). However, our understanding of the molecular mechanisms controlling gut inflammation remains insufficient, hindering the development of targeted therapies for IBD and CRC. In this study, we uncovered *C15ORF48/miR-147* as a negative regulator of gut inflammation, operating through the modulation of epithelial cell metabolism. *C15ORF48/miR-147* encodes two molecular products, C15ORF48 protein and miR-147-3p microRNA, which are predominantly expressed in the intestinal epithelium. *C15ORF48/miR-147* ablation leads to gut dysbiosis and exacerbates chemically induced colitis in mice. C15ORF48 and miR-147-3p work together to suppress colonocyte metabolism and inflammation by silencing *NDUFA4*, a subunit of mitochondrial complex IV (CIV). Interestingly, the C15ORF48 protein, a structural paralog of NDUFA4, contains a unique C-terminal α-helical domain crucial for displacing NDUFA4 from CIV and its subsequent degradation. *NDUFA4* silencing hinders NF-κB signaling activation and consequently attenuates inflammatory responses. Collectively, our findings have established the *C15ORF48/miR-147-NDUFA4* molecular axis as an indispensable regulator of gut homeostasis, bridging mitochondrial metabolism and inflammation.

C15ORF48/miR-147 | NDUFA4 | gut inflammation | mitochondrial metabolism | microbiome

Aberrant inflammation plays a central role in the pathogenesis of various gastrointestinal (GI) diseases, including inflammatory bowel disease (IBD) and colorectal cancer (CRC). Although broad immunosuppressive strategies, such as TNFα or IL-12 inhibition, provide treatment options for IBD, their considerable side effects and limited efficacy highlight the need for improved, more specific therapies (1, 2). To enable the informed development of innovative targeted therapies for the treatment of IBD and CRC, a deeper understanding of the mechanisms regulating gut inflammation and mucosal immunity is required.

Unlike most other animal organs, gut tissue exists in a state of persistent, low-grade inflammation due to constant exposure to luminal microbiota (3). This "physiological" inflammatory environment in the gut necessitates the existence of a complex and highly nuanced control mechanism to prevent "pathological" inflammatory responses. The gut epithelium, consisting of a single layer of intestinal epithelial cells (IECs), is a cornerstone of this exquisite regulatory apparatus (4). Besides maintaining a direct barrier function, IECs also play an integral role in various aspects of the inflammatory response, including i) sensing of commensals and pathogens, ii) context-dependent regulation of tissue-resident immune cell responses, iii) elimination of invading pathogens, and iv) resolution of inflammation and tissue repair (5–9). Moreover, IECs shape the composition of gut microbiota by promoting the growth of some microbes and inhibiting others (10). Conversely, gut microbiota can modulate epithelial and immune cell responses through the production of various metabolites (11).

Increasing evidence suggests that reprogramming of mitochondrial metabolism plays an important role in the regulation of intestinal inflammation and microbiome homeostasis (12). During gut inflammation, the metabolic program of IECs undergoes significant changes to meet the high energy and nutrient demands of the immune response and tissue repair processes: IECs throttle down energy generation through oxidative phosphorylation (OXPHOS) and concomitantly increase the utilization of anaerobic glycolysis (9, 13). In addition, the altered mitochondrial activity of inflamed IECs results in the production of various metabolites such as reactive oxygen species (ROS) and succinate, which activate NF-κB signaling and promote inflammation (14). Interestingly, it has been postulated that

Significance

Emerging evidence emphasizes the significance of mitochondrial metabolism reprograming in the gut epithelium for regulating intestinal inflammation. Nevertheless, the intricate mechanisms underpinning this connection remain elusive. We have uncovered the predominant expression of *C15ORF48/miR-147* in the gut epithelium and conducted an in vivo investigation of its functions. Our findings suggest that epithelial *C15ORF48/miR-147* safeguards against aberrant gut inflammation and dysbiosis. Mechanistically, through its two molecular products—C15ORF48 protein and miR-147-3p miRNA—*C15ORF48/miR-147* silences *NDUFA4*, a mitochondrial complex IV subunit. Notably, NDUFA4 not only impacts mitochondrial respiration but also controls inflammation signaling. This establishes the *C15ORF48/miR-147-NDUFA4* molecular axis as an essential controller of gut homeostasis, linking energy metabolism and inflammation. These insights hold promise for innovative therapies against gastrointestinal diseases.

The authors declare no competing interest.

This article is a PNAS Direct Submission.

Copyright © 2024 the Author(s). Published by PNAS. This article is distributed under Creative Commons Attribution-NonCommercial-NoDerivatives License 4.0 (CC BY-NC-ND).

[1]To whom correspondence may be addressed. Email: mboldin@coh.org.

This article contains supporting information online at https://www.pnas.org/lookup/suppl/doi:10.1073/pnas.2315944121/-/DCSupplemental.

Published June 25, 2024.

mitochondrial dysfunction in IECs is a crucial driver in the pathogenesis of IBD, supporting the notion that changes in mitochondrial metabolism can directly shape the inflammatory response (12). Despite significant progress in the field, the precise molecular mechanisms through which mitochondria function as a central signaling hub in regulating intestinal inflammation remain inadequately understood.

In this study, we test the hypothesis that *C15ORF48/miR-147* functions as a critical regulator of gut inflammation by controlling mitochondrial metabolism. *C15ORF48/miR-147* is an inflammation-induced gene that produces two distinct molecular products: a small mitochondrial protein, C15ORF48, and a microRNA, miR-147-3p (15). These two molecules work cooperatively to regulate cell metabolism and inflammation by inhibiting *NDUFA4*, an accessory subunit of the mitochondrial complex IV (CIV) (16, 17). However, the role of *C15ORF48/miR-147* in inflammation remains controversial with some studies suggesting that it serves as an inflammation promoter (17), whereas others indicate an inhibitory role (16). Furthermore, the physiological role of *C15ORF48/miR-147* remains unclear due to the lack of appropriate animal models for testing its function.

Our findings using mouse genetic models suggest that *C15ORF48/miR-147* is highly expressed in IECs under physiological conditions and functions as a molecular brake on intestinal inflammation by silencing *NDUFA4* and subsequently dampening mitochondrial metabolism.

Results

***C15ORF48/miR-147* Is Predominantly Expressed in IECs.** Our initial interest in *C15ORF48/miR-147* stems from its role as the miR-147-3p host gene. This miRNA was originally identified as a lipopolysaccharide (LPS)-inducible miRNA that attenuates inflammatory responses in myeloid cells (15). However, prior efforts did not fully establish the physiological functions of this miRNA. In addition to miR-147-3p, its host gene is predicted to give rise to a small (83aa) protein, C15ORF48, which shares a high degree (53% similarity) of sequence homology with NDUFA4 protein (*SI Appendix*, Fig. S1 *A* and *B*). NDUFA4 was recently identified as the 14th subunit of the mitochondrial CIV and proposed to regulate CIV homodimerization (18, 19). *NDUFA4* knockdown (KD) in mammalian cells attenuates CIV activity and inhibits proliferation in cells dependent on OXPHOS as their only energy source (19). Interestingly, miR-147-3p is predicted by the TargetScan algorithm to bind to the 3′UTR of *NDUFA4* and attenuate its expression (20, 21) (*SI Appendix*, Fig. S1*C*).

To start defining the physiological functions of *C15ORF48/miR-147,* we performed expression profiling of several mouse tissues. Our qRT-PCR analysis of mature miR-147-3p expression (Fig. 1*A*) and western blot analysis of C15ORF48 expression (Fig. 1*B*) suggest that both molecular products of *C15ORF48/miR-147* are predominantly expressed in the large intestine. Furthermore, immunofluorescence analysis of mouse colon tissue sections indicates that C15ORF48 is primarily expressed by $EpCAM^+$ IECs (Fig. 1*C*). Interestingly, C15ORF48 is mainly expressed by terminally differentiated colonocytes in the apical part of the crypt structures, whereas the intestinal stem cells and proliferating progenitors at the base of the crypts are apparently devoid of C15ORF48 expression (*SI Appendix*, Fig. S2*A*), suggesting that *C15ORF48/miR-147* may have a role in colonocyte differentiation and/or its expression is potentially controlled by a protein or chemical gradient along the apical–basal axis (22–24). In addition, our immunofluorescence analysis of human colon carcinoma HCT116 cells revealed that C15ORF48 protein is colocalized with a classical mitochondrial marker TOMM20 (*SI Appendix*, Fig. S2*B*), suggesting that C15ORF48 is a mitochondrial protein. This observation is in good agreement with prior findings (16). Based on the data from the Genotype-Tissue Expression (GTEx) portal (https://gtexportal.org/) and the Human Protein Atlas (https://www.proteinatlas.org), the expression pattern of human *C15ORF48/miR-147* is largely congruent with the mouse expression profile (Fig. 1*D* and *SI Appendix*, Fig. S2*C*), indicating possible evolutionary conservation of *C15ORF48/miR-147* functions in IECs.

Mitochondrial dysfunction in colonocytes is implicated as a disease driver in ulcerative colitis (UC) patients (25–27). Thus, to explore the potential role of *C15ORF48/miR-147* in aberrant gut inflammation, we examined the expression levels of *C15ORF48/miR-147* in rectal mucosal biopsies isolated from new-onset UC patients (GSE109142) (25) and found a significant *C15ORF48/miR-147* down-regulation in comparison to normal controls (Fig. 1*E*), suggesting a potential role for *C15ORF48/miR-147* in the pathogenesis of IBD.

Epithelial *C15ORF48/miR-147* Protects Mice from Dextran Sodium Sulfate (DSS)-Induced Colitis. To genetically dissect the functions of *C15ORF48/miR-147*, we generated germline *C15ORF48/miR-147* knockout (KO) mice (hereafter *C15ORF48/miR-147*$^{-/-}$ mice) that lack expression of both C15ORF48 and miR-147-3p in all tissues. This was accomplished by deleting a ~2 kb genomic fragment that encompasses exons 4 and 5 of *C15ORF48/miR-147* using CRISPR/Cas9 gene editing technology (*SI Appendix*, Fig. S3*A*). The loss of *C15ORF48/miR-147* expression in the KO mice was verified by western blot analysis using anti-mouse C15ORF48 antibody (*SI Appendix*, Fig. S3*B*) and qRT-PCR analysis of miR-147-3p (*SI Appendix*, Fig. S3*C*). *C15ORF48/miR-147*$^{-/-}$ mice develop normally and do not display any overt morphological changes in the gut (*SI Appendix*, Fig. S3*E*). Of note, our analysis of the major immune cell populations in *C15ORF48/miR-147*$^{-/-}$ mice using flow cytometry also did not reveal any gross defects (*SI Appendix*, Fig. S3 *G* and *H*).

To examine the role of *C15ORF48/miR-147* in gut inflammation, we challenged *C15ORF48/miR-147*$^{-/-}$ mice with DSS to induce acute colitis. The DSS-induced colitis mouse model was chosen in part because it resembles the pathophysiological features of human UC (28), which as discussed above displays *C15ORF48/miR-147* dysregulation (Fig. 1*E*). Consistent with the reduced expression of *C15ORF48/miR-147* observed in human UC patients, we found a decrease in C15ORF48 protein levels in the colons of DSS-challenged C57BL6/J mice (*SI Appendix*, Fig. S3*F*). Upon DSS administration, *C15ORF48/miR-147*$^{-/-}$ mice develop an exacerbated colitis, as indicated by more profound body weight loss (Fig. 2*A*), an elevated disease activity index (DAI) (29) (Fig. 2*B*), more pronounced shortening of the colon (Fig. 2*C*), and considerably higher colon permeability (Fig. 2*D*) in comparison to wild-type (WT) control mice. Histopathological analysis of colon tissue from DSS-challenged *C15ORF48/miR-147*$^{-/-}$ mice revealed a more severe disease in comparison to the control, as indicated by more extensive gland loss, epithelial layer erosion, edema, and immune cell infiltration (Fig. 2 *E* and *F*). Furthermore, based on immunofluorescence analysis of colon sections, *C15ORF48/miR-147*$^{-/-}$ mice display a significant decrease in IEC proliferation and a remarkable accumulation of $CD45^+$ immune cells (Fig. 2*G*). Additionally, production of proinflammatory cytokines, such as IL6, was significantly up-regulated in *C15ORF48/miR-147*$^{-/-}$ colons (Fig. 2*H*). Together, our findings demonstrate that *C15ORF48/miR-147* is required to keep gut inflammation in check.

To determine whether aberrant inflammation in *C15ORF48/miR-147*$^{-/-}$ mice is driven by a defect in the immune or epithelial cells

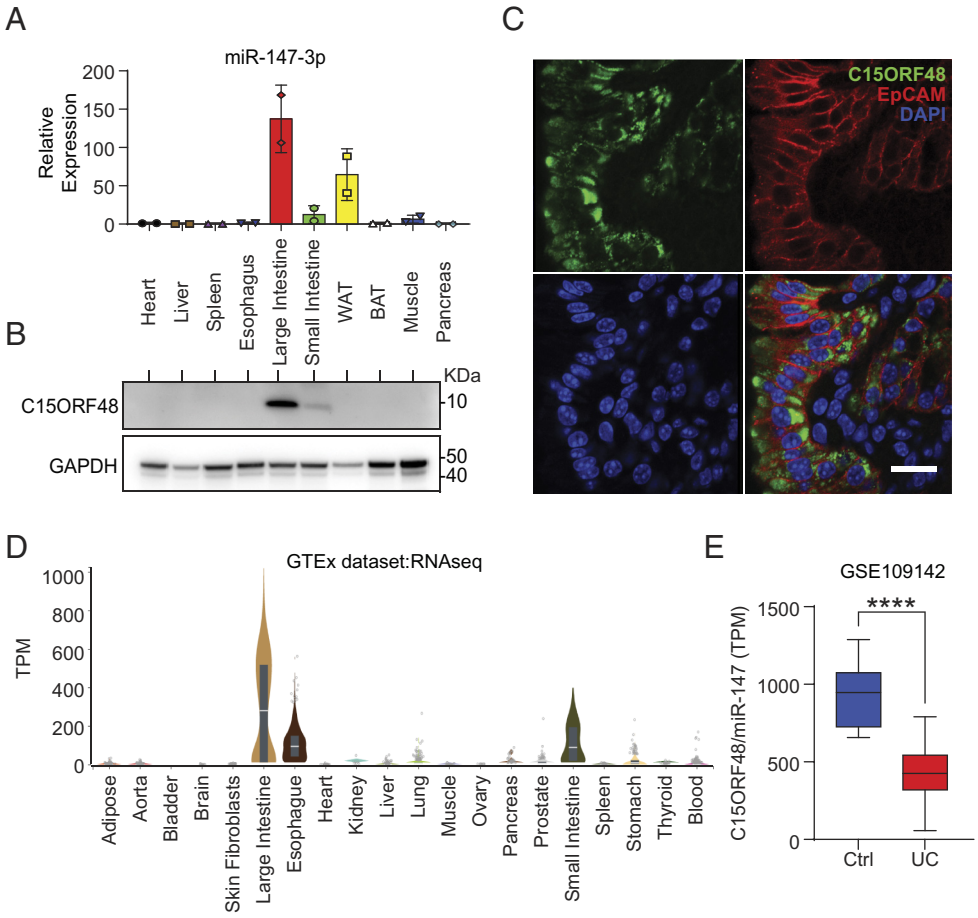

Fig. 1. The *C15ORF48/miR-147* gene encodes two distinct molecular products—miR-147-3p miRNA and C15ORF48 protein—both of which are abundantly expressed in the large intestine. (*A*) qRT-PCR analysis of mature miR-147-3p expression in various tissues isolated from C57BL/6J mice (n = 2), including the heart, liver, spleen, esophagus, large intestine, small intestine, white adipose tissue (WAT), brown adipose tissue (BAT), muscle, and pancreas. The expression levels were normalized to snoRNA234, and miR-147-3p expression in the heart was arbitrarily set to 1. (*B*) Western blot (WB) analysis of C15ORF48 protein expression in different tissues isolated from the C57BL/6J mouse. GAPDH serves as loading control. (*C*) Immunofluorescence (IF) analysis of C15ORF48 (green) and EpCAM (epithelial cell marker, red) expression in mouse colon tissue. DAPI stain (blue) was used to define nuclei. (Scale bar, 10 μm.) (*D*) Violin plot of *C15ORF48/miR-147* expression in normal human tissues. The data were compiled by querying the GTEx portal (https://gtexportal.org). Expression values are shown in transcripts per million reads (TPM). (*E*) *C15ORF48/miR-147* expression in rectal mucosal biopsies from healthy controls (n = 20) and new-onset pediatric ulcerative colitis patients (n = 206). The previously published GSE109142 dataset (25) was used for the analysis. Expression values are shown in TPM reads. ****$P < 0.0001$ by Student's *t* test. Data in (*A*), (*D*), and (*E*) are shown as mean ± SD.

of the gut, we generated bone marrow (BM) chimeric mice (*SI Appendix*, Fig. S4*A*) and challenged them with DSS. We found that *C15ORF48/miR-147*$^{-/-}$ hosts develop more severe colitis than WT hosts regardless of the source of donor BM as indicated by more pronounced body weight loss (*SI Appendix*, Fig. S4*B*), colon shortening (*SI Appendix*, Fig. S4*C*), and epithelial layer erosion (*SI Appendix*, Fig. S4*D*), suggesting that nonimmune (most likely epithelial) *C15ORF48/miR-147* plays a protective role in gut inflammation. Interestingly, *C15ORF48/miR-147* in immune cells might have an inflammation promoting role because *C15ORF48/miR-147*$^{-/-}$ host mice transplanted with *C15ORF48/miR-147*$^{-/-}$ BM (KO→KO chimera) displayed less severe weight loss than *C15ORF48/miR-147*$^{-/-}$ host mice transplanted with WT BM (WT→KO chimera) (*SI Appendix*, Fig. S4*B*).

To more precisely define the cell-intrinsic role of *C15ORF48/miR-147* in gut inflammation, we generated mice with an IEC-specific *C15ORF48/miR-147* deletion. To that end, we first made a conditional *C15ORF48/miR-147* allele (hereafter *C15ORF48/miR-147*$^{fl/fl}$) by inserting two *loxP* sites flanking exons 4 and 5 of the *C15ORF48/miR-147* gene using CRISPR/Cas9 technology (*SI Appendix*, Fig. S3 *A* and *J*). Like *C15ORF48/miR-147*$^{-/-}$ mice, *C15ORF48/miR-147*$^{fl/fl}$ mice are predicted to abrogate expression of both C15ORF48 and miR-147-3p after *Cre*-mediated locus excision. *C15ORF48/miR-147*$^{fl/fl}$ mice were then crossed with *Villin1-Cre* (*Vil1*^{Cre}) deleter mice (30) to generate *Vil1*^{Cre}*C15ORF48/miR-147*$^{fl/fl}$ (hereafter *C15ORF48/miR-147*$^{\Delta IEC}$) mice. *Villin1* encodes an actin-binding protein whose expression is restricted to gut and renal epithelial cells (30). As expected, *C15ORF48/miR-147*$^{\Delta IEC}$ mice display an IEC-specific loss of C15ORF48 (*SI Appendix*, Fig. S3*I*). In agreement with our BM chimera studies, DSS challenge of *C15ORF48/miR-147*$^{\Delta IEC}$ mice results in a more severe colitis in comparison with control *Vil1*^{Cre} mice (Fig. 2 *I*–*K*). Thus, our mouse genetic studies establish *C15ORF48/miR-147* as an essential, IEC-intrinsic negative regulator of gut inflammation.

***C15ORF48/miR-147* Deletion Up-Regulates IEC Metabolism and Inflammatory Responses.** To define the molecular mechanism by which *C15ORF48/miR-147* controls gut inflammation, we performed global transcriptome analysis of purified *C15ORF48/miR-147*-sufficient and -deficient colonocytes from unchallenged and DSS-challenged mice using RNA-seq. We found that *C15ORF48/miR-147* ablation alters expression of 128 genes in cells from unchallenged mice (*SI Appendix*, Fig. S5*A*) and 1,039 genes in the colonocytes from DSS-challenged mice (*SI Appendix*, Fig. S5*C*). Pathway analysis of differentially expressed genes (DEGs) in untreated *C15ORF48/miR-147*$^{-/-}$ colonocytes identified a

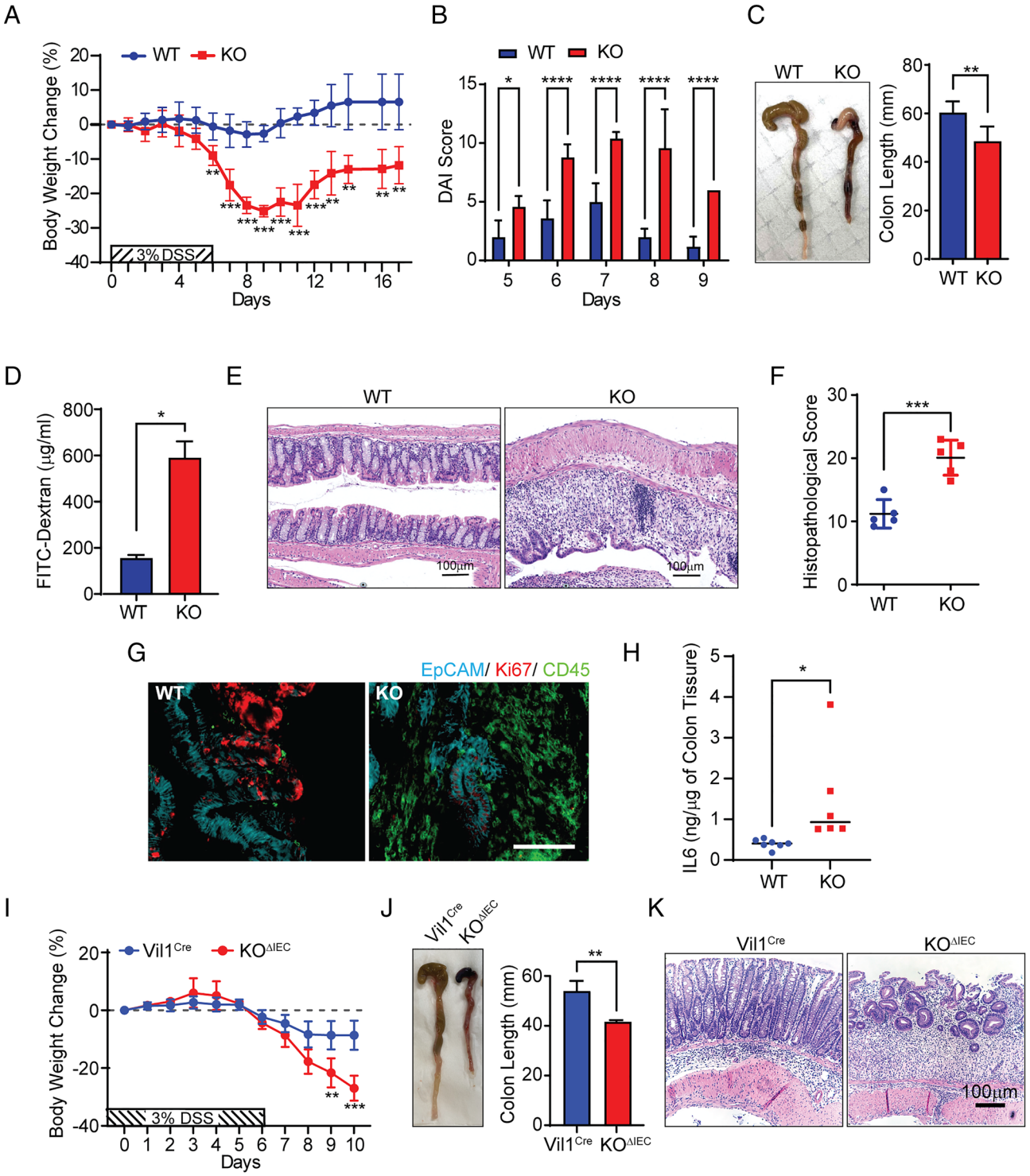

Fig. 2. Epithelial *C15ORF48/miR-147* protects mice from fulminant DSS-induced colitis. (*A*) Body weight change in WT and *C15ORF48/miR-147*$^{-/-}$ (KO) mice (n = 5) challenged with 3% DSS for 6 d. (*B*) DAI in WT and *C15ORF48/miR-147*$^{-/-}$ (KO) mice (n = 5) challenged with 3% DSS for 6 d. The DAI was calculated on days 5 to 9 after the start of the DSS treatment as a sum of the body weight decrease, stool consistency, and rectal bleeding scores (0 to 4 scale). (*C*) Representative image of the colons and colon length in WT and *C15ORF48/miR-147*$^{-/-}$ (KO) mice on day 10 after 3% DSS treatment (n = 5). (*D*) Analysis of colon permeability in WT and *C15ORF48/miR-147*$^{-/-}$ (KO) mice on day 9 after 3% DSS challenge (n = 2). Serum concentrations of FITC-Dextran were determined 4 h after the oral administration of the compound. (*E*) Representative images of H&E-stained colon tissue sections from WT and *C15ORF48/miR-147*$^{-/-}$ (KO) mice on day 10 after 4% DSS treatment. Note a more profound epithelial erosion, loss of glands, and infiltration of lymphoid cells in the KO sample. (Scale bar, 100 μm.) (*F*) Histopathology scores for WT and *C15ORF48/miR-147*$^{-/-}$ (KO) mice on day 10 of the DSS-induced colitis model (n = 5). The score is a sum of the severity scores (0 to 5 scale) for gland loss, epithelial erosion, epithelial hyperplasia, edema, lymphoid accumulation, inflammation, and neutrophil infiltration. (*G*) IF analysis of EpCAM (cyan), Ki67 (proliferation marker; red), and CD45 (immune cell marker; green) expression in colon tissue sections isolated from WT and *C15ORF48/miR-147*$^{-/-}$ (KO) mice on day 9 of the DSS-induced colitis model. Note a lack of epithelial cell proliferation and massive recruitment of immune cells in the KO samples. (*H*) ELISA analysis of IL6 production in colon homogenate samples from WT and *C15ORF48/miR-147*$^{-/-}$ (KO) mice on day 9 of the DSS-induced colitis model. IL6 concentration is normalized to tissue weight. (*I*) Body weight change and (*J*) colon length in control Vil1^{Cre} and *C15ORF48/miR-147*$^{\Delta IEC}$ (KO$^{\Delta IEC}$) mice (n = 5) after 3% DSS challenge for 6 d. (*K*) H&E-stained colon tissue sections from control Vil1^{Cre} and KO$^{\Delta IEC}$ mice at day 10 of the DSS-induced colitis model. (Scale bar, 100 μm.) Data in (*A–D*), (*F*), (*H–J*) panels are shown as mean ± SD. *P < 0.05; **P < 0.01; ***P < 0.001; ****P < 0.0001 by Student's t test.

significant up-regulation of genes involved in inflammatory responses (type I and II IFN signaling) and energy metabolism (OXPHOS, glycolysis, and xenobiotic metabolism) (Fig. 3*A*). Mirroring the untreated cells, the DSS-challenged *C15ORF48/miR-147*$^{-/-}$ colonocytes exhibited an up-regulation of innate immune (type I IFN, IL6 and TNF receptor pathways) and cellular metabolism (OXPHOS, mTOR signaling, and xenobiotic metabolism) genes (Fig. 3 *D* and *E*). We validated the aberrant activation of inflammatory responses in DSS-challenged *C15ORF48/miR-147*$^{-/-}$ colonocytes using qRT-PCR analysis of the proinflammatory cytokine IL1β (Fig. 3*F*).

To further investigate the role of *C15ORF48/miR-147* in energy metabolism, we examined the rates of OXPHOS and anaerobic glycolysis in the purified *C15ORF48/miR-147*-sufficient and -deficient colonocytes using Seahorse extracellular flux technology. We observed that oxygen consumption rates (OCRs) associated with both basal and maximal mitochondrial respiration were significantly elevated in *C15ORF48/miR-147*$^{-/-}$ colonocytes (Fig. 3*B* and *SI Appendix*, Fig. S5 *D* and *E*). Moreover, extracellular acidification rates (ECARs), which measure lactic acid levels generated during anaerobic glycolysis, were also significantly higher in *C15ORF48/miR-147*$^{-/-}$ cells (*SI Appendix*, Fig. S5 *B, F,* and *G*). However, the baseline OCR/ECAR ratio is lower in *C15ORF48/miR-147*$^{-/-}$ colonocytes (Fig. 3*C*), suggesting that *C15ORF48/miR-147* deletion not only elevates the overall metabolic potential of IECs but also skews their energy metabolism

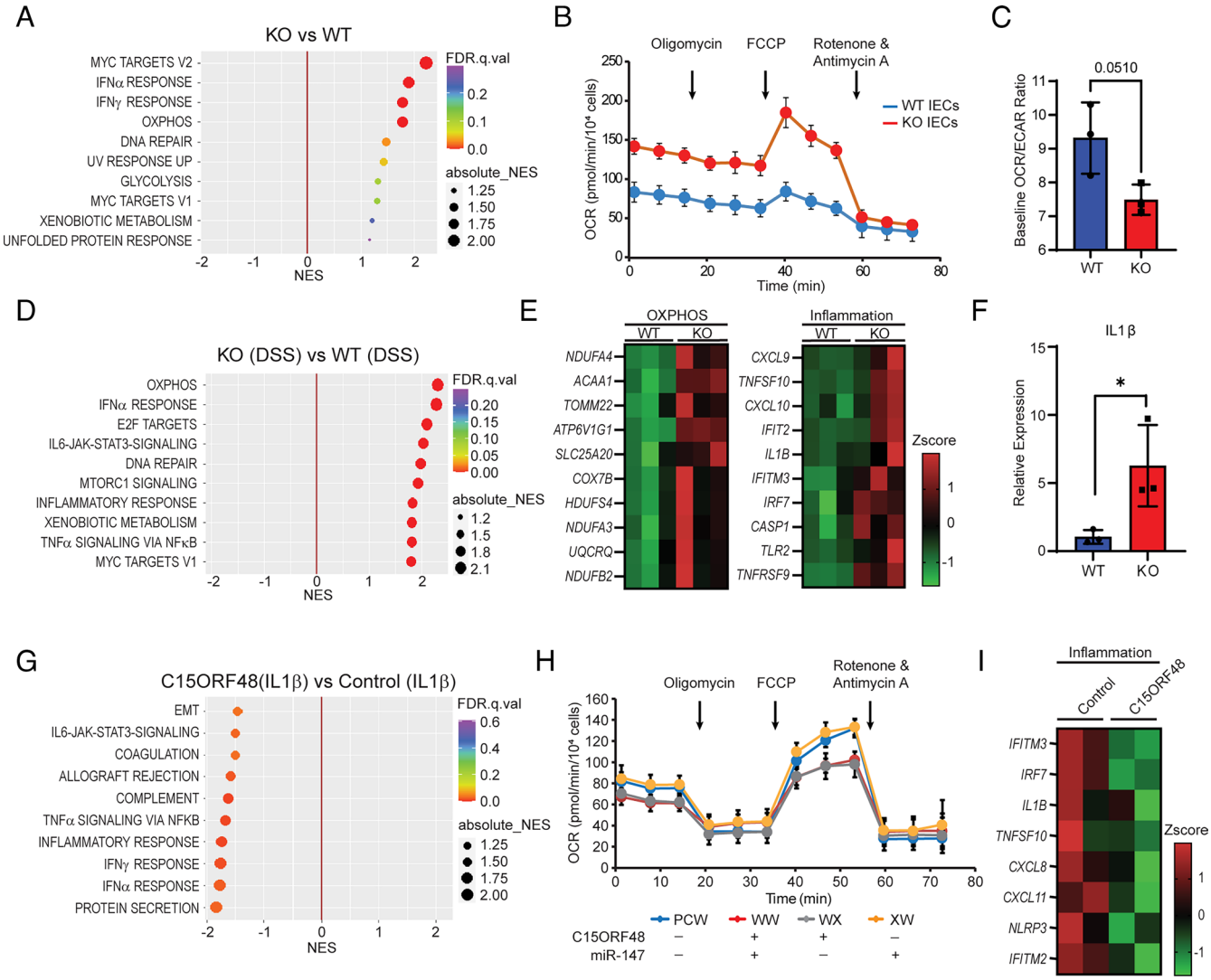

Fig. 3. Loss of *C15ORF48/miR-147* results in the dysregulation of inflammatory signaling and metabolic activities in colonocytes. (*A*) GSEA pathway enrichment analysis of up-regulated genes (fold change >1.5; $P < 0.05$; RPKM > 1) in unchallenged *C15ORF48/miR-147*$^{-/-}$ (KO) colonocytes. WT colonocytes served as the baseline to determine the DEGs in KO colonocytes. NES, normalized enrichment score. (*B*) OCR profiles of purified primary colonocytes isolated from WT and *C15ORF48/miR-147*$^{-/-}$ (KO) mice. The OCRs were measured sequentially under basal conditions, following inhibition of ATP synthase (with oligomycin), uncoupling the ETC with FCCP, and blocking complex I and III with rotenone and antimycin, respectively. The data were normalized using cell counts per well. (*C*) Baseline OCR to ECAR ratio of purified colonocytes isolated from WT and *C15ORF48/miR-147*$^{-/-}$ (KO) mice (n = 3). $P = 0.051$ by Student's *t* test. (*D*) GSEA pathway enrichment analysis of up-regulated genes (fold change >1.5; $P < 0.05$; RPKM > 1) in DSS-challenged (3% for 3 d) *C15ORF48/miR-147−/−* (KO) colonocytes. WT colonocytes served as the baseline to determine the DEGs in KO colonocytes. NES, normalized enrichment score. (*E*) Heatmap of gene expression values (z-score normalization) for several selected OXPHOS (*Left*) and inflammation-related (*Right*) genes in WT and *C15ORF48/miR-147*$^{-/-}$ (KO) colonocytes (n = 3) after 3 d DSS challenge. (*F*) qRT-PCR analysis of *IL1β* expression in purified colonocytes isolated from WT and *C15ORF48/miR-147*$^{-/-}$ (KO) mice after 3 d DSS challenge (n = 3). *GAPDH* was used for normalization. *$P < 0.05$ by Student's *t* test. (*G*) GSEA pathway enrichment analysis of down-regulated genes (fold change < −1.5; $P < 0.05$; RPKM > 1) in IL1β (100 ng/mL for 4 h) challenged HCT116 cells ectopically expressing FLAG-tagged C15ORF48 protein. NES, normalized enrichment score. (*H*) OCR profiles of HCT116 cells stably expressing tetracycline-inducible pCW57.1-*C15ORF48/miR-147* expression constructs. PCW is a vector control; WW plasmid gives rise to both C15ORF48 and miR-147-3p; WX plasmid was engineered to produce C15ORF48 alone; XW plasmid was engineered to produce miR-147-3p alone. (*I*) Heatmap of gene expression values (z-score normalization) for several selected inflammation-related genes in IL1β (100 ng/mL for 4 h) challenged HCT116 cells ectopically expressing FLAG-tagged C15ORF48 protein. Data in (*B*), (*C*), (*F*), and (*H*) panels are shown as mean ± SD.

toward glycolysis, a metabolic switch that is often observed during inflammation (31–33).

To dissect the role of C15ORF48 and miR-147-3p in the regulation of energy metabolism, we generated the *C15ORF48/miR-147* expression constructs (Fig. 4*B*) that encode either C15ORF48 alone (WX construct) or miR-147-3p alone (XW construct) and compared their impact on mitochondrial respiration with *C15ORF48/miR-147* cDNA (WW construct) that encodes both molecular products. First, we found that *C15ORF48/miR-147* (WW construct) overexpression in gut epithelial and macrophage cell lines dampens their energy metabolism by attenuating both OXPHOS and anaerobic glycolysis (Fig. 3*H* and *SI Appendix*, Figs. S5*J* and S6). This finding is directly opposite to our observations with *C15ORF48/miR-147*$^{-/-}$ colonocytes (Fig. 3*B* and *SI Appendix*, Fig. S5*B*). Additionally, both C15ORF48 and miR-147-3p can lower the ECAR, whereas the maximal OCR is significantly attenuated only by C15ORF48 (WX construct), but not miR-147-3p (XW construct) (Fig. 3*H* and *SI Appendix*, Fig. S5*J*). Collectively, these findings demonstrate that C15ORF48 and miR-147-3p function as suppressors of energy metabolism but have distinct roles in this inhibitory process.

In addition, we observed that C15ORF48 protein overexpression down-regulates genes involved in the regulation of energy metabolism and inflammation. Gene set enrichment analysis (GSEA) (34)

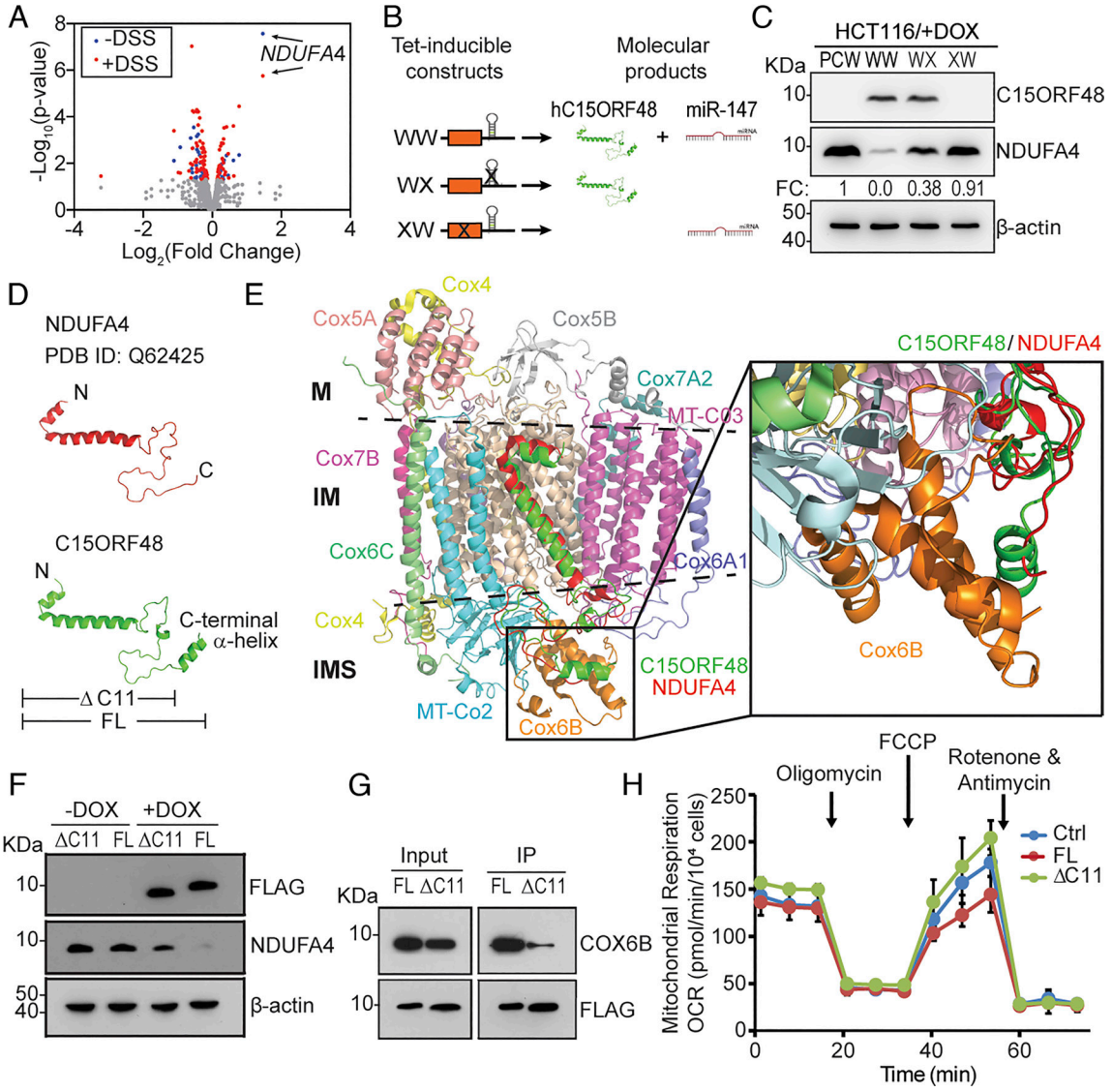

Fig. 4. C15ORF48 and miR-147-3p cooperatively suppress *NDUFA4* in colonocytes. (*A*) Volcano plot showing expression changes for putative miR-147-3p target genes in purified colonocytes isolated from unchallenged (blue) and DSS-challenged (3% DSS for 3 d) (red) WT and *C15ORF48/miR-147*$^{-/-}$ (KO) mice (n = 3). Note *NDUFA4* as the most significantly induced miR-147-3p target under both conditions. (*B*) Schematic diagram of tetracycline-inducible pCW57.1-*C15ORF48/miR-147* expression plasmids and their corresponding molecular products. *C15ORF48/miR-147* cDNA was mutated to direct differential expression of C15ORF48 and miR-147-3p. WW gives rise to both C15ORF48 and miR-147-3p; WX produces C15ORF48 alone; XW produces miR-147-3p alone. (*C*) WB analysis of NDUFA4 and C15ORF48 expression in HCT116 cells stably expressing tetracycline-inducible pCW57.1-*C15ORF48/miR-147* expression constructs. Relative NDUFA4 expression was calculated using densitometry and normalized to β-actin levels. NDUFA4 expression in empty vector cells (PCW) was arbitrarily set to 1. FC: fold change. Note a strong capacity of the WX construct (C15ORF48 alone) to suppress NDUFA4 expression. (*D*) The comparison of the predicted structure of C15ORF48 (green) and the crystal structure of NDUFA4 (red) (PDB ID: Q62425). Note a unique C-terminal α-helix in C15ORF48. FL: full-length C15ORF48; ΔC11: truncated version of C15ORF48 that lacks the C-terminal α-helix (11aa). (*E*) The relative positions of NDUFA4 (red) and C15ORF48 (green) in CIV cryo-EM structure (PDB ID: 5Z62). All CIV subunits are depicted in tube representation. Note the close proximity of the C-terminal α-helix of C15ORF48 to COX6B subunit, shown in the magnified *Inset*. (*F*) WB analysis of HCT116 cells expressing tetracycline-inducible FLAG-tagged C15ORF48 or its ΔC11 mutant using anti-FLAG and anti-NDUFA4 antibodies. β-actin was used for normalization. (*G*) Coimmunoprecipitation of endogenous COX6B with FLAG-tagged C15ORF48 proteins isolated from HCT116 cell mitochondria. (*H*) OCR profiles of HCT116 cells expressing tetracycline-inducible FLAG-tagged C15ORF48 or its ΔC11 mutant. Cells were induced with doxycycline for 48 h before the analysis. Note an elevated mitochondrial respiration in ΔC11 OE HCT116 cells. Data are shown as mean ± SD. DOX, doxycycline.

of DEGs in unstimulated C15ORF48 overexpressing (OE) cells revealed a down-regulation of cell metabolism (OXPHOS and glycolysis) pathways (*SI Appendix*, Fig. S5 *H* and *I*), while down-regulated transcripts in IL1β stimulated C15ORF48 OE cells were enriched in inflammatory response genes (type I and II IFN, TNF, and IL6 signaling) (Fig. 3 *G* and *I*). Of note, these findings are opposite to gene expression changes observed in *C15ORF48/miR-147*-deficient colonocytes (Fig. 3 *A* and *D*). Collectively, the opposite gene expression changes observed in *C15ORF48/miR-147*-deficient colonocytes and C15ORF48 OE cells suggest that *C15ORF48/miR-147* may function as a negative regulator of inflammation and cell metabolism.

Cooperative Action of C15ORF48 and miR-147-3p Silences *NDUFA4*. To further understand the molecular mechanisms of *C15ORF48/miR-147*, we examined the impact of its ablation on putative miR-147-3p targets. Our analysis of DEGs in *C15ORF48/miR-147*$^{-/-}$ colonocytes suggests that *NDUFA4* is the only miR-147-3p target gene (out of 1,070 putative targets) that is significantly up-regulated with or without the DSS challenge (Fig. 4*A*). Moreover, we also detected an elevated NDUFA4 expression by western blot analysis of total colon extracts and purified colonocytes from *C15ORF48/miR-147*$^{-/-}$ mice (*SI Appendix*, Fig. S3*D*). Using a 3′UTR luciferase reporter assay, we confirmed the capacity of miR-147-3p to attenuate *NDUFA4* expression by binding directly to an evolutionarily conserved "seed" sequence in the 3′UTR of *NDUFA4* (*SI Appendix*, Fig. S7*A*).

In line with these findings, we observed that *C15ORF48/miR-147* overexpression suppresses NDUFA4 protein expression (Fig. 4*C* and *SI Appendix*, Fig. S7*C*); however, this effect is more profound than the typical mild effect of miRNA-mediated regulation. Therefore, to further understand the NDUFA4 silencing capacity of *C15ORF48/miR-147*, we made use of the *C15ORF48/miR-147* expression mutants (WW, WX, and XW constructs; Fig. 4*B*) that combinatorially express C15ORF48 and miR-147-3p molecules and were discussed above. Our analysis revealed that C15ORF48 protein has a stronger capacity to down-regulate NDUFA4, in comparison to miR-147-3p (Fig. 4*C* and *SI Appendix*, Fig. S7*C*). In contrast to miR-147-3p, C15ORF48 has no destabilizing effect on *NDUFA4* mRNA (*SI Appendix*, Fig. S7*D*), suggesting that C15ORF48 triggers NDUFA4 protein degradation. We found that C15ORF48-mediated NDUFA4 degradation is proteasome independent because proteasomal inhibitors do not interfere with the process (*SI Appendix*, Fig. S7*E*). Taken together, our results imply that miR-147-3p and C15ORF48 act cooperatively to silence NDUFA4 at the posttranscriptional and posttranslational levels, respectively.

Because NDUFA4 and C15ORF48 proteins display significant sequence homology, we used the PyMOL algorithm to compare the predicted secondary structure of C15ORF48 with the deposited crystal structure of NDUFA4 (Fig. 4*D*) and docked both molecules into the published crystal structure of mitochondrial CIV (Fig. 4*E*). Our results indicate that the N-terminal portions of C15ORF48 and NDUFA4, which comprise the transmembrane domains of both proteins, are superimposable, suggesting the same docking position of C15ORF48 and NDUFA4 in CIV. On the other hand, C15ORF48 has a unique α-helical domain in its C terminus, which is positioned in close proximity to the COX6B subunit of CIV (Fig. 4*E*).

To investigate the role of the C-terminal α-helix in C15ORF48, we generated a truncated version of C15ORF48 that lacks this structural moiety (ΔC11 construct; Fig. 4*D*). Our immunofluorescence analysis suggests that deletion of the C-terminal α-helix has no impact on mitochondrial localization of C15ORF48 (*SI Appendix*, Fig. S7*F*) but interferes with the capacity of C15ORF48 to induce NDUFA4 protein degradation (Fig. 4*F* and *SI Appendix*, Fig. S7*G*). These results indicate that the C-terminal α-helical domain in C15ORF48 is required for NDUFA4 degradation. In agreement with our modeling studies (Fig. 4*E*), immunoprecipitation experiments revealed that the C-terminal α-helical domain in C15ORF48 is responsible for its interaction with the COX6B subunit of CIV (Fig. 4*G*). However, the significance of this interaction for C15ORF48 function is currently unclear. Additionally, in contrast to the full-length C15ORF48, overexpression of the ΔC11 mutant elevates mitochondrial respiration (Fig. 4*H*) and boosts the metabolic potential (*SI Appendix*, Fig. S7*H*) of colonocytes.

***NDUFA4* Depletion Attenuates Cellular Metabolism and Inflammation.** Our findings indicate that *C15ORF48/miR-147* functions by suppressing *NDUFA4*; however, the role of *NDUFA4* in the regulation of gut inflammation is unclear. Thus, to facilitate our analysis of *NDUFA4* functions, we silenced its expression in HCT116 cells using CRISPR/Cas9 gene editing technology. As expected, western blot analysis of several independent *NDUFA4* KO clones revealed a complete loss of NDUFA4 expression (*SI Appendix*, Fig. S8*A*). In line with previous reports suggesting a role for *NDUFA4* in the regulation of CIV activity (19), baseline and maximal mitochondrial respiration were significantly attenuated in *NDUFA4* KO cells (Fig. 5*A* and *SI Appendix*, Fig. S8*B*). As a result, *NDUFA4* KO cells become more glycolytic; however, their overall metabolic potential is reduced in comparison to control cells (*SI Appendix*, Fig. S8*C*). Similar trends were observed in RAW264.7 *NDUFA4* KD macrophages (*SI Appendix*, Fig. S9 *A–C*), suggesting that the impact of *NDUFA4* on mitochondrial respiration is tissue independent.

Global transcriptome analysis of *NDUFA4* KO cells revealed perturbed expression of 2,010 genes in untreated cells (*SI Appendix*, Fig. S8*D*) and 2,217 genes upon IL1β challenge (*SI Appendix*, Fig. S8*E*). GSEA analysis of the DEGs identified a significant down- regulation of genes controlling inflammatory responses and hypoxia in both unstimulated (*SI Appendix*, Fig. S8*F*) and IL1β challenged *NDUFA4* KO cells (Fig. 5*B*). Defective activation of inflammatory responses was also observed in LPS-treated RAW264.7 *NDUFA4* KD cells (*SI Appendix*, Fig. S9 *D–G*), suggesting that control of inflammatory signaling by *NDUFA4* is global and stimulus independent. We further examined the impact of *NDUFA4* depletion on the activation of diverse signaling pathways in response to inflammatory stimuli and concluded that *NDUFA4* promotes a broad range of innate immune effector responses, including proinflammatory cytokine and chemokine secretion (TNFα and CXCL8; Fig. 5*C* and *SI Appendix*, Fig. S9*H*), dsRNA sensing and IFN signaling (OAS1; Fig. 5*C*), ROS generation, and nitric oxide (NO) production (NOS2; Fig. 5*C* and *SI Appendix*, Fig. S9 *I* and *J*). Furthermore, we observed a notable reduction of IκBα phosphorylation and subsequent IκBα degradation in *NDUFA4*-depleted cells (Fig. 5*D* and *SI Appendix*, Fig. S9*K*). In line with these findings, activation of an NF-κB luciferase reporter was significantly diminished in *NDUFA4* KO cells (Fig. 5*E*). Taken together, these observations indicate that *NDUFA4* depletion leads to a substantial attenuation of NF-κB activation, which might contribute to the profound dysregulation of inflammatory signaling in these cells. Our findings also imply a potential role for *NDUFA4* as a molecular link between mitochondrial metabolism and inflammation. Additionally, the opposite direction of energy metabolism and inflammatory response changes in *C15ORF48* OE and *NDUFA4* KO cells on one hand, and *C15ORF48/miR-147* KO cells, on the other, supports our hypothesis that *C15ORF48/miR-147* negatively regulates cell metabolism and inflammation by suppressing *NDUFA4*.

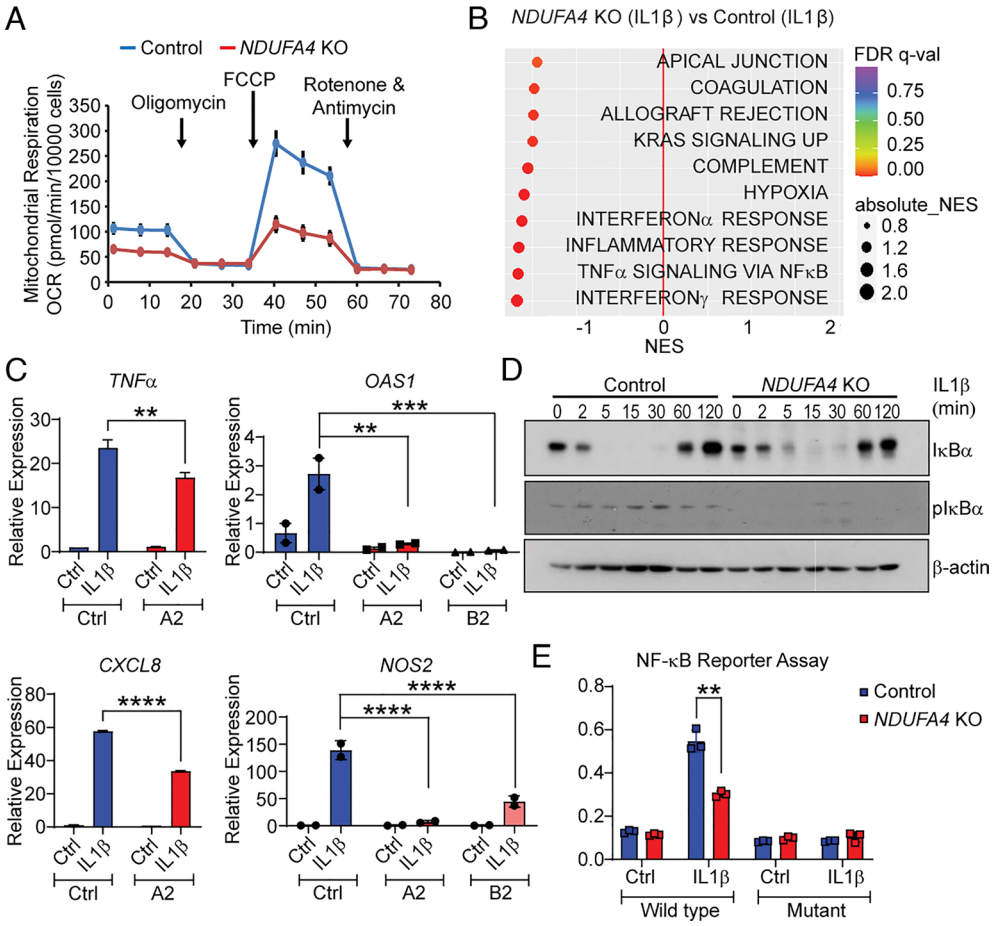

Fig. 5. *NDUFA4* is an essential positive regulator of energy metabolism and inflammation. (*A*) OCR profile of *NDUFA4* KO (A2 clone) HCT116 cells. Control, parental HCT116 cells. (*B*) GSEA analysis of down-regulated genes (fold change < −1.5; $P < 0.05$; RPKM > 1) in IL1β (100 ng/mL for 4 h) challenged *NDUFA4* KO (A2 and B2 clones) cells. NES, normalized enrichment score. (*C*) qRT-PCR analysis of *TNFα*, *CXCL8*, *OAS1*, and *NOS2* expression in unchallenged and IL1β (100 ng/mL for 4 h) challenged parental control and *NDUFA4* KO cells (A2 and B2 clones). *GAPDH* was used for normalization. Gene expression values in untreated parental control cells were arbitrarily set to 1. (*D*) WB analysis of IL1β (100 ng/mL for indicated time) stimulated parental control and *NDUFA4* KO cells (A2 clone) using anti-phospho-IκBα and anti-total IκBα antibodies. β-actin was used as loading control. (*E*) Analysis of NF-κB activation in unstimulated and IL1β (100 ng/mL for 6 h) stimulated parental control and *NDUFA4* KO cells (A2 clone) using NF-κB luciferase reporter assay. WT Firefly luciferase reporter contains three consensus NF-κB binding sites, which are mutated in the mutant reporter. Cotransfected *Renilla* luciferase reporter (pRL-SV40) was used for normalization. Data in (*A*), (*C*), and (*E*) are shown as mean ± SD. $^{**}P < 0.01$; $^{***}P < 0.005$; $^{****}P < 0.0001$ using one-way ANOVA.

The Ability of C15ORF48 to Control Cell Metabolism and Inflammation Is Limited to Its NDUFA4 Silencing Capacity. The capability of *C15ORF48/miR-147* to silence *NDUFA4* and the structural homology between C15ORF48 and NDUFA4 proteins raise a possibility that C15ORF48 can replace NDUFA4 in CIV and, thus, specifically reshape CIV activity. To test this notion, we ectopically expressed FLAG-tagged C15ORF48 and its ΔC11 mutant in *NDUFA4* KO cells (*SI Appendix*, Fig. S10*A*). Interestingly, the maximal mitochondrial respiration capacity of *NDUFA4* KO cells expressing the full-length C15ORF48 was not substantially altered (Fig. 6*A* and *SI Appendix*, Fig. S10*B*), indicating that C15ORF48 cannot fully rescue the impaired OXPHOS in *NDUFA4* KO cells Fig. 5*A*. In contrast, the ΔC11 mutant significantly elevated the maximal respiration in *NDUFA4* KO cells, suggesting that it can functionally substitute NDUFA4 in CIV (Fig. 6*A* and *SI Appendix*, Fig. S10*B*). As control, overexpression of FLAG-tagged NDUFA4 also rescued the OXPHOS defect in *NDUFA4* KO cells (Fig. 6*A* and *SI Appendix*, Fig. S10*B*). Collectively, these findings support a hypothesis that the principal function of C15ORF48 is NDUFA4 silencing, and the C-terminal α-helical domain is critical for this activity. Deletion of the C-terminal moiety seems to transform C15ORF48 into an NDUFA4 functional homolog. This conclusion is further supported by our finding that ΔC11 mutant OE boosts the metabolic potential of *NDUFA4*-sufficient cells (Fig. 4*H*).

We also examined how overexpression of the full-length C15ORF48 and its ΔC11 mutant impacts inflammation signaling in *NDUFA4* KO cells. In contrast to a complete rescue of IL1β-driven activation of *OAS1* and *NOS2* by NDUFA4 (*SI Appendix*, Fig. S10*C*), we observed a partial rescue of *OAS1* by both C15ORF48 and ΔC11 mutant, whereas the induction of *TNFα* and *NOS2* was not significantly affected (Fig. 6*B* and *SI Appendix*, Fig. S10*D*). The specific rescue of the mitochondrial respiration defect, but not the innate immune defect by ΔC11 mutant OE in *NDUFA4* KO cells indicates that the *C15ORF48/miR-147-NDUFA4* axis regulates inflammation and cell metabolism through different mechanisms (*SI Appendix*, Fig. S10*E*).

Gut Dysbiosis Mediates Fulminant Colitis in *C15ORF48/miR-147*$^{-/-}$ Mice. Because the gut microbiota plays an important role in the pathogenesis of inflammatory GI diseases (35, 36), we examined how changes in gut microbiota impact aberrant inflammation in *C15ORF48/miR-147*$^{-/-}$ mice. To this end, *C15ORF48/miR-147*$^{-/-}$ and WT mice were treated with broad-spectrum antibiotics for 4 wk and then challenged with DSS. Analysis of body weight changes revealed no significant protection against excessive inflammation in WT mice (Fig. 7*A*). Furthermore, cohousing of *C15ORF48/miR-147*$^{-/-}$ and WT mice for 4 wk yielded a similar experimental outcome (Fig. 7*B*), suggesting that gut dysbiosis is potentially mediating fulminant colitis in *C15ORF48/miR-147*$^{-/-}$ mice. To determine the underlying dysbiotic changes, we performed 16S ribosomal RNA gene sequencing (16S rRNA-seq) of fecal DNA isolated from separately housed *C15ORF48/miR-147*$^{-/-}$ and WT mice. Unsupervised principal coordinates analysis (PCoA) of Bray–Curtis distance indicated that *C15ORF48/miR-147*$^{-/-}$ and WT microbiomes are very dissimilar (different beta diversity) (Fig. 7*C*). In contrast, no significant difference ($P = 0.92$) in the Shannon diversity index (alpha diversity; measures microbiome heterogeneity in each mouse strain) was observed (*SI Appendix*, Fig. S11*A*). Application of the Linear discriminant analysis Effect Size (LEfSe) method to define the most significant taxonomic changes in the two mouse strains, revealed just five operational taxonomic units (OTUs) (*Lachnospiraceae_NK4A136, Dubosiella, Eubacterium xylanophilum, Turicibacter,* and *Blautia*) that are significantly

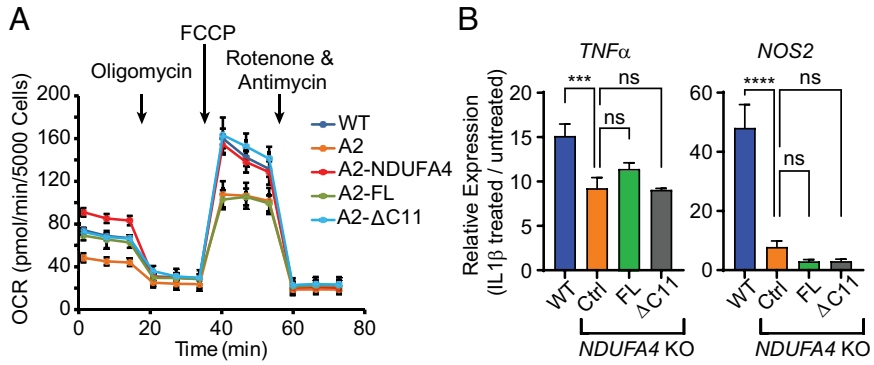

Fig. 6. C15ORF48 overexpression is unable to fully rescue the metabolic and inflammatory defects in *NDUFA4* KO colonocytes. (*A*) OCR profiles of *NDUFA4* KO (clone A2) cells stably expressing FLAG-tagged NDUFA4, FLAG-tagged full-length C15ORF48 (FL), and its ΔC11 mutant. WT, parental HCT116 cells; A2, *NDUFA4* KO (clone A2) cells. (*B*) qRT-PCR analysis of *TNFα* and *NOS2* expression in unchallenged and IL1β (100 ng/mL for 4 h) challenged *NDUFA4* KO cells OE FLAG-tagged full-length C15ORF48 (FL) and its ΔC11 mutant. *GAPDH* was used for normalization. Gene expression in untreated HCT116 cells (WT) was arbitrarily set to 1. Ctrl, *NDUFA4* KO (clone A2) cells. Data are shown as mean ± SD. ns, no significance; ***$P < 0.005$; ****$P < 0.0001$ using one-way ANOVA.

decreased in *C15ORF48/miR-147*$^{-/-}$ mice (Fig. 7*D* and *SI Appendix*, Fig. S11*B*). The first three OTUs on this list are relatively abundant and comprise close to 20% of the WT gut microbiome (*SI Appendix*, Fig. S11 *B* and *C*). In *C15ORF48/miR-147*$^{-/-}$ mice, the relative abundance of these OTUs plummets ~10-fold. The bacteria in the five OTUs are obligate anaerobes and belong to the *Firmicutes* phylum, which is known to play a protective, anti-inflammatory role in the gut (37–39). Of note, the *Firmicutes* to *Bacteroidetes* abundance ratio in *C15ORF48/miR-147*$^{-/-}$ mice is trending lower (~50% drop; *SI Appendix*, Fig. S11*D*), mirroring findings observed in IBD patients (40). Because the most significant taxonomic changes in the *C15ORF48/miR-147*$^{-/-}$ microbiome were depletions of bacterial OTUs rather than expansions, it is unlikely that fecal transfer of bacteria from *C15ORF48/miR-147*$^{-/-}$ mice to cohoused WT mice can explain the exacerbation of colitis phenotype in WT mice after cohabitation. Alternatively, this observation suggests that a transfer of microbiota-shaping metabolites or bacteriophages, rather than the bacteria itself, triggers dysbiosis and subsequently drives severe colitis in cohoused WT mice.

Discussion

Despite recent recognition of *C15ORF48/miR-147* as an important innate immunity regulator, its precise contributions to host homeostasis and inflammatory responses remain controversial and poorly understood. Here, we report that *C15ORF48/miR-147* is abundantly expressed in IECs and functions as an essential cell-intrinsic regulator of gut inflammation and microbiome homeostasis. These functions of *C15ORF48/miR-147* are mechanistically linked to its capacity to regulate mitochondrial metabolism at least in part by controlling *NDUFA4*, an auxiliary subunit of mitochondrial CIV. In line with these observations, we found that depletion of *NDUFA4* in IECs results in attenuation of energy metabolism and inflammatory signaling. Collectively, our genetic studies establish the *C15ORF48/miR-147-NDUFA4* molecular axis as an important regulator of cellular metabolism and intestinal homeostasis (*SI Appendix*, Fig. S12).

Our findings indicate that *C15ORF48/miR-147* acts as a negative regulator of inflammation because its genetic ablation strongly exacerbates DSS-induced colitis in mice. Our results are in good

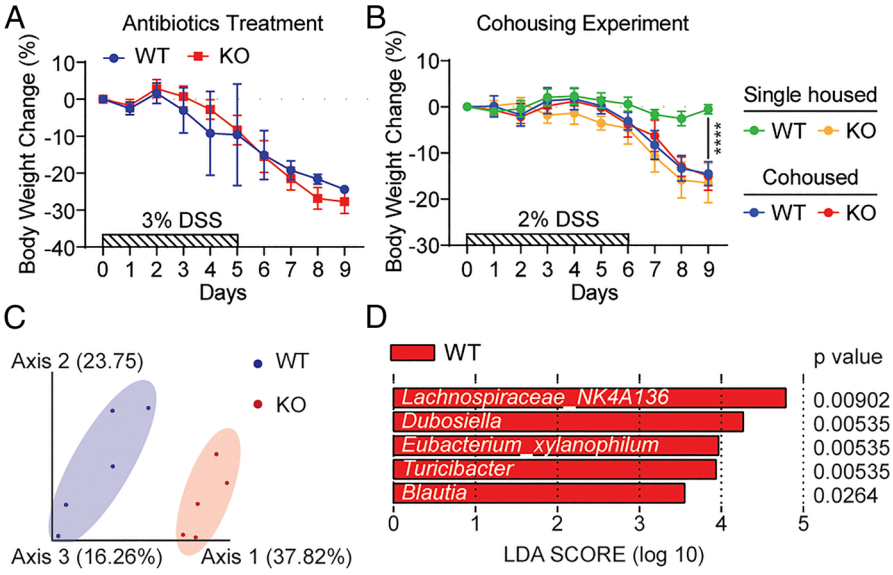

Fig. 7. Gut dysbiosis mediates severe colitis in *C15ORF48/miR-147*$^{-/-}$ mice. (*A*) Body weight changes in antibiotic-treated WT and *C15ORF48/miR-147*$^{-/-}$ (KO) mice (n = 5) upon DSS challenge. Mice were treated with broad-spectrum antibiotics (ampicillin: 1 g/L; neomycin: 1 g/L; metronidazole: 1 g/L; vancomycin: 0.25 g/L) in drinking water for 4 wk before colitis induction (3% DSS treatment for 5 d). (*B*) Body weight changes in single-house and cohoused WT and *C15ORF48/miR-147*$^{-/-}$ (KO) mice (n = 5) upon DSS challenge. After being cohoused for 4 wk, mice were subsequently separated by their genotypes prior to inducing colitis using a 2% DSS treatment for 6 d. (*C*) Unsupervised PCoA of Bray–Curtis distance between WT and *C15ORF48/miR-147*$^{-/-}$ (KO) fecal microbiomes (n = 5). (*D*) Linear discriminant analysis Effect Size (LEfSe) of significant taxonomic changes (LDA score > 2, $P < 0.05$) between WT and *C15ORF48/miR-147*$^{-/-}$ (KO) microbiomes. LDA, linear discriminant analysis. Data in (*A*) and (*B*) are shown as mean ± SD. ****$P < 0.0001$ by one-way ANOVA.

agreement with a previous in vitro report demonstrating an anti-inflammatory role of *C15ORF48/miR-147* in human aortic endothelial cells during viral infection (16). Conversely, Clayton et al. reported that *C15ORF48/miR-147* can promote inflammation in primary human macrophages in response to LPS (17). These incongruous findings indicate that *C15ORF48/miR-147* might play distinct roles in innate immune responses depending on the cellular context and/or inflammatory stimulus. Indeed, our BM transplantation experiments provide support for this notion: we found that *C15ORF48/miR-147* in nonhematopoietic cells (most likely IECs) protects mice from aberrant gut inflammation, whereas immune *C15ORF48/miR-147,* in contrast, promotes it. Nevertheless, further research using conditional KO mice will be required to confirm the tissue-specific functional duality of *C15ORF48/miR-147* in inflammation.

We posit that *C15ORF48/miR-147* elicits its regulatory functions in gut inflammation primarily by silencing *NDUFA4*. The two distinct molecular products of *C15ORF48/miR-147*—C15ORF48 protein and miR-147-3p miRNA—act cooperatively to posttranscriptionally suppress *NDUFA4*. Several lines of evidence support this hypothesis. First, analysis of *C15ORF48/miR-147* KO colonocytes revealed significant up-regulation of *NDUFA4* mRNA and protein expression. Importantly, *NDUFA4* was the only putative miR-147-3p target that was derepressed in *C15ORF48/miR-147* KO colonocytes. Second, *C15ORF48/miR-147* overexpression in HCT116 colonocytes drives profound *NDUFA4* suppression, which is largely elicited by C15ORF48-mediated NDUFA4 protein degradation. In addition, we established *NDUFA4* as a bona fide miR-147-3p target using the 3′UTR luciferase assay; however, the contribution of miR-147-3p to NDUFA4 down-regulation is relatively minor in comparison with C15ORF48, in line with the fine-tuning role typically ascribed to miRNAs. Third, we found that gene expression changes, including down-regulation of proinflammatory and mitochondrial metabolism signaling, in *NDUFA4* KO IECs are very congruent to the gene expression changes in C15ORF48-expressing cells that undergo a marked NDUFA4 silencing. On the other hand, *C15ORF48/miR-147* KO colonocytes display an up-regulation of proinflammatory and mitochondrial metabolism genes that is nicely correlated with the observed *NDUFA4* derepression in these cells. The notion of *NDUFA4* as a principal target of *C15ORF48/miR-147* is also supported by the findings of two other reports that were published while our study was in preparation (16, 17). Despite the accumulating evidence of the importance of the *C15ORF48/miR-147-NDUFA4* molecular axis, our data do not completely rule out the possibility that *C15ORF48/miR-147* has additional targets through which it elicits its regulatory functions in the gut and other tissues. It is worth noting in this regard that miR-147-3p was previously reported to target *HOXC6* and *SLC22A3*, and thus suppress cell proliferation and inflammatory responses, respectively (41, 42).

Our analysis of C15ORF48-mediated NDUFA4 silencing suggests that this process is transcription independent and does not require proteasomal activity. Furthermore, we found that a unique C-terminal α-helical domain that is present in C15ORF48 but not in its NDUFA4 paralog is necessary to trigger NDUFA4 degradation. Thus, we hypothesize that the incorporation of structurally distinct C15ORF48 paralog into mitochondrial CIV potentially displaces the NDUFA4 subunit and makes it susceptible for a protease attack. The nature of the protease that degrades NDUFA4 and the mechanism of its activation is currently unclear. However, the mitochondrion is known to harbor a number of organelle-specific mitoproteases, some of which (e.g., OMA1 and LONP1) were previously implicated in the control of NDUFA4 expression under stress conditions (43, 44).

The ability of C15ORF48 protein to potentially replace NDUFA4 in CIV raises a possibility that such paralog swap may result in the formation of a non-canonical CIV with distinct metabolic properties. Indeed, we and others have found that C15ORF48 overexpression results in significant dampening of mitochondrial OXPHOS (16). However, it is not clear from these experiments whether this energy metabolism change is driven by the incorporation of C15ORF48 into CIV or is simply the consequence of NDUFA4 loss. To address this question, we ectopically expressed C15ORF48 in *NDUFA4*-deficient IECs and found a partial restoration of the OXPHOS defect, specifically improving basal mitochondrial respiration capacity, while the maximal respiration capacity remained impaired in the reconstituted cells. Moreover, C15ORF48 overexpression also failed to rescue the compromised inflammatory responses in NDUFA4-depleted cells. Thus, our results suggest that the incorporation of C15ORF48 into mitochondrial CIV has limited effect on its activity and indicate that the principal function of C15ORF48 is the control of *NDUFA4* expression. Besides, these findings provide additional support for the notion that NDUFA4 is the primary target through which *C15ORF48/miR-147* mediates its control of mitochondrial metabolism and inflammatory responses.

Growing evidence suggests that *NDUFA4* plays an important role in regulating CIV activity and by this virtue in controlling mitochondrial respiration (16, 19). However, its role and the mechanisms of action in regulating innate immune responses are still poorly understood. Loss of *NDUFA4* in human-induced pluripotent stem cells was recently shown to induce mitochondrial stress, leading to mitochondrial DNA leakage and up-regulation of type I interferon responses (45). In our study, we found that *NDUFA4* deletion in human IECs and mouse macrophages impairs activation of inflammatory responses, including production of mitochondrial ROS, nitric oxide, and proinflammatory cytokines. We also observed a significant defect in NF-κB activation in *NDUFA4* KO cells that could explain the dysregulated innate immune responses. One hypothetical mechanism through which *NDUFA4* can control activation of inflammatory signaling is the generation of immunomodulatory metabolites. For example, the dysregulation of CIV activity due to *NDUFA4* loss may result in the accumulation of ROS, which is known to promote LPS-induced NF-κB activation and proinflammatory cytokine release (14). Indeed, we observed that *NDUFA4* KD macrophages treated with LPS display a defect in ROS production, which becomes apparent several hours post-stimulation and, therefore, is unlikely to mediate the NF-κB activation defect that has a much faster kinetic. In addition, our data suggest that overexpression of ΔC11 mutant (NDUFA4 mutant lacking C-terminal α-helix) in *NDUFA4* KO IECs can effectively rescue the OXPHOS defect but has no effect on the impaired cytokine production in these cells, implying that the control of CIV activity and inflammation by *NDUFA4* is mechanistically decoupled. Hypothetically, NDUFA4 might be directly involved in the activation of proinflammatory signaling by signal-induced translocation to the cytoplasm and triggering of NF-κB signaling via the inflammasome or IKK complex activation. Small mitochondrial proteins, for example, cytochrome C and DELE1, were shown to translocate to the cytoplasm to activate proapoptotic signaling and signal mitochondrial stress, respectively (46, 47).

C15ORF48/miR-147 was originally described as an inflammation-induced gene. However, we found it to be constitutively expressed in the intestinal epithelium, most likely because the gut exists in the state of low-grade, "physiological" inflammation due to constant exposure to the luminal microbiota. Moreover, our immunofluorescence analysis suggests that C15ORF48 is abundantly expressed in the apical epithelium but is absent in the deep crypt pockets of the mouse colon. This expression pattern may be attributed to the fact that apical

colonocytes in contrast to crypt colonocytes are more exposed to the luminal bacteria. Alternatively, an increase in C15ORF48 expression in colon epithelium along the crypt–villus axis may indicate a role for *C15ORF48/miR-147* in IEC differentiation: the crypt usually contains stem cells and undifferentiated colonocytes, whereas the apical epithelium is composed of fully matured colonocytes. This notion is supported by a previous report suggesting that miR-147-3p OE suppresses stem-like properties of colon cancer cells (48).

The *C15ORF48/miR-147* gene gives rise to two molecular products—C15ORF48 and miR-147-3p—from the same RNA transcript. However, the biogenesis of mature miR-147-3p with its two endonuclease cleavage events likely renders the rest of the *C15ORF48/miR-147* mRNA unsuitable for efficient C15ORF48 translation due to a poly-A tail loss and subsequent transcript degradation. Because we found that colonocytes express C15ORF48 along with miR-147-3p, we hypothesize the existence of two separate pools of *C15ORF48/miR-147* transcripts: one that gives rise to miR-147-3p and another one that produces C15ORF48. Furthermore, the differential expression of these two molecules in the small intestine (exclusive C15ORF48 expression) and adipose tissues (only miR-147-3p expressed) (Fig. 1 *A* and *B*) suggests the presence of a regulatory mechanism that can control selective production of C15ORF48 and miR-147-3p molecules. Given our observation that C15ORF48 and miR-147-3p have distinct roles in the regulation of mitochondrial metabolism, selective expression of these two molecules might be linked to the tissue's metabolic status.

Our findings imply a link between gut dysbiosis and the development of severe DSS-induced colitis in *C15ORF48/miR-147* KO mice. We observed that WT mice cohoused with *C15ORF48/miR-147* KO mice exhibited a more severe colitis compared to single-housed WT mice, suggesting transmission of the fulminant colitis phenotype from *C15ORF48/miR-147* KO to WT mice during cohabitation. Notably, we found that the trait transmission occurred prior to colitis development because cohoused WT and *C15ORF48/miR-147* KO mice were kept separately after the DSS challenge. In line with these findings, microbiome analysis revealed significant dissimilarities in the fecal bacterial communities of WT and *C15ORF48/miR-147* KO mice. Surprisingly, the five significantly different bacterial OTUs (*Lachnospiraceae*_NK4A136, *Dubosiella*, *Eubacterium xylanophilum*, *Turicibacter*, and *Blautia*) were more abundant in WT mice in comparison with *C15ORF48/miR-147* KO mice. Thus, a fecal transfer of bacteria from *C15ORF48/miR-147* KO to WT mice cannot possibly explain the development of severe colitis phenotype in WT mice after cohabitation. An alternative hypothesis that potentially can explain our mouse cohousing experiments is the fecal transfer of microbiome-shaping metabolites or specific bacteriophages from *C15ORF48/miR-147* KO to WT mice. Fecal volatile organic compounds (VOCs) resulting from the metabolic activities of the intestinal mucosa and gut microbiota have been reported to contribute to GI disorders and response to treatment in IBD (49, 50). For instance, IBD patients exhibit elevated phenol concentrations in fecal samples compared to healthy controls. High phenol levels promote inflammation and induce proinflammatory cytokine production in murine macrophages. Therefore, fecal VOCs or other metabolites could potentially be responsible for the dysbiosis in *C15ORF48/miR-147* KO mice and drive severe colitis in WT mice upon transfer from *C15ORF48/miR-147* KO mice during the cohabitation.

In summary, our results have established the *C15ORF48/miR-147* as a critical regulator of gut inflammation and microbiome homeostasis. *C15ORF48/miR-147* mediates its function by controlling mitochondrial metabolism through *NDUFA4* silencing. However, our study not only uncovered an elegant regulatory circuit that connects cellular metabolism and intestinal inflammation but may also open broad avenues for targeted therapies in autoimmune and other GI diseases.

Materials and Methods

Details about the generation of *C15ORF48/miR-147*$^{-/-}$ and *C15ORF48/miR-147*$^{fl/fl}$ mice are provided in *SI Appendix, Materials and Methods*. Mouse genotyping using genomic PCR, cell culture, generation of anti-mouse C15ORF48 antibody, induction and clinical evaluation of DSS-induced colitis, colon permeability assay, flow cytometry, histopathological analysis, immunofluorescence analysis, ELISA, colonocyte isolation, Seahorse extracellular flux assay, western blot analysis, bone marrow transplantation, gene expression plasmids, generation of *NDUFA4* knockout and knockdown cells, lentiviral production and transduction, dual-luciferase reporter assay, RNA isolation and qRT-PCR, global transcriptome profiling by RNA-seq, coimmunoprecipitation experiments, total ROS measurement, mouse microbiota depletion with antibiotic treatment, mouse cohousing experiments, fecal microbiome analysis, and statistical analysis were performed according to the protocols described in *SI Appendix, Materials and Methods*.

Data, Materials, and Software Availability. The source data for RNA-Seq have been deposited in the NCBI Gene Expression Omnibus (GEO) database (accession number: GSE246492 and GSE246493) (51).

ACKNOWLEDGMENTS. This study was funded in part by the National Institute of Allergy and Infectious Diseases of the NIH R01 AI125615 (to M.P.B.) and R01 AI146313 (to M.P.B.) grants and City of Hope Shared Resources Pilot grant. Research reported in this publication includes work performed in the Analytical Cytometry, Integrative Genomics and Veterinary Pathology Cores supported by the National Cancer Institute of the NIH under the P30 CA033572 award (to City of Hope Comprehensive Cancer Center). The funders had no role in study design, data collection and analysis, decision to publish, or preparation of the manuscript. We thank Dr. Walter Tsark from the Transgenic Mouse core of City of Hope for the assistance with generating the *C15ORF48/miR-147*$^{-/-}$ and *C15ORF48/miR-147*$^{fl/fl}$ mice. We also thank Drs. Xiwei Wu and Wei Chen from the Integrative Genomics core of City of Hope for help with the RNA-seq analysis.

Author affiliations: [a]Department of Systems Biology, Beckman Research Institute, City of Hope, Duarte, CA 91010; [b]Department of Biochemistry and Molecular Medicine, Keck School of Medicine, University of Southern California, Los Angeles, CA 90033; and [c]Department of Pharmacology, School of Pharmacy, China Pharmaceutical University, Nanjing, Jiangsu 210009, China

Author contributions: M.X., Z.L., W.-L.W., and M.P. B. designed research; M.X., Z.L., B.W., and T.S. performed research; M.X. contributed new reagents/analytic tools; M.X., Z.L., N.G., and M.C. analyzed data; and M.X. and M.P.B. wrote the paper.

1. L. Peyrin-Biroulet, Anti-TNF therapy in inflammatory bowel diseases: A huge review. *Minerva Gastroenterol. Dietol.* **56**, 233–243 (2010).
2. S. Danese, New therapies for inflammatory bowel disease: From the bench to the bedside. *Gut.* **61**, 918–932 (2012).
3. C. Fiocchi, Intestinal inflammation: A complex interplay of immune and nonimmune cell interactions. *Am. J. Physiol.* **273**, G769–G775 (1997).
4. L. W. Peterson, D. Artis, Intestinal epithelial cells: Regulators of barrier function and immune homeostasis. *Nat. Rev. Immunol.* **14**, 141–153 (2014).
5. S. Al-Ghadban, S. Kaissi, F. R. Homaidan, H. Y. Naim, M. E. El-Sabban, Cross-talk between intestinal epithelial cells and immune cells in inflammatory bowel disease. *Sci. Rep.* **6**, 29783 (2016).
6. C. Pardo-Camacho, A. M. Gonzalez-Castro, B. K. Rodino-Janeiro, M. Pigrau, M. Vicario, Epithelial immunity: Priming defensive responses in the intestinal mucosa. *Am. J. Physiol. Gastrointest. Liver Physiol.* **314**, G247–G255 (2018).
7. G. Roda *et al.*, Intestinal epithelial cells in inflammatory bowel diseases. *World J. Gastroenterol.* **16**, 4264–4271 (2010).
8. M. F. Kagnoff, The intestinal epithelium is an integral component of a communications network. *J. Clin. Invest.* **124**, 2841–2843 (2014).
9. J. M. Allaire *et al.*, The intestinal epithelium: Central coordinator of mucosal immunity. *Trends Immunol.* **39**, 677–696 (2018).
10. R. Okumura, K. Takeda, Roles of intestinal epithelial cells in the maintenance of gut homeostasis. *Exp. Mol. Med.* **49**, e338 (2017).

11. H. Tilg, N. Zmora, T. E. Adolph, E. Elinav, The intestinal microbiota fuelling metabolic inflammation. *Nat. Rev. Immunol.* **20**, 40–54 (2020).
12. E. A. Novak, K. P. Mollen, Mitochondrial dysfunction in inflammatory bowel disease. *Front. Cell Dev. Biol.* **3**, 62 (2015).
13. E. Rath, D. Haller, Intestinal epithelial cell metabolism at the interface of microbial dysbiosis and tissue injury. *Mucosal. Immunol.* **15**, 595–604 (2022).
14. M. J. Morgan, Z. G. Liu, Crosstalk of reactive oxygen species and NF-kappaB signaling. *Cell Res.* **21**, 103–115 (2011).
15. G. Liu *et al.*, miR-147, a microRNA that is induced upon Toll-like receptor stimulation, regulates murine macrophage inflammatory responses. *Proc. Natl. Acad. Sci. U.S.A.* **106**, 15819–15824 (2009).
16. C. Q. E. Lee *et al.*, Coding and non-coding roles of MOCCI (C15ORF48) coordinate to regulate host inflammation and immunity. *Nat. Commun.* **12**, 2130 (2021).
17. S. A. Clayton *et al.*, Inflammation causes remodeling of mitochondrial cytochrome c oxidase mediated by the bifunctional gene C15orf48. *Sci. Adv.* **7**, eabl5182 (2021).
18. S. Zong *et al.*, Structure of the intact 14-subunit human cytochrome c oxidase. *Cell Res.* **28**, 1026–1034 (2018).
19. E. Balsa *et al.*, NDUFA4 is a subunit of complex IV of the mammalian electron transport chain. *Cell Metab.* **16**, 378–386 (2012).
20. B. P. Lewis, C. B. Burge, D. P. Bartel, Conserved seed pairing, often flanked by adenosines, indicates that thousands of human genes are microRNA targets. *Cell* **120**, 15–20 (2005).
21. V. Agarwal, G. W. Bell, J. W. Nam, D. P. Bartel, Predicting effective microRNA target sites in mammalian mRNAs. *Elife* **4**, e05005 (2015).
22. B. B. Madison *et al.*, Epithelial hedgehog signals pattern the intestinal crypt-villus axis. *Development* **132**, 279–289 (2005).
23. H. Tian *et al.*, Opposing activities of Notch and Wnt signaling regulate intestinal stem cells and gut homeostasis. *Cell Rep.* **11**, 33–42 (2015).
24. L. Zheng, C. J. Kelly, S. P. Colgan, Physiologic hypoxia and oxygen homeostasis in the healthy intestine. A Review in the Theme: Cellular responses to hypoxia. *Am. J. Physiol. Cell Physiol.* **309**, C350–C360 (2015).
25. Y. Haberman *et al.*, Ulcerative colitis mucosal transcriptomes reveal mitochondriopathy and personalized mechanisms underlying disease severity and treatment response. *Nat. Commun.* **10**, 38 (2019).
26. H. Li, L. Lai, J. Shen, Development of a susceptibility gene based novel predictive model for the diagnosis of ulcerative colitis using random forest and artificial neural network. *Aging (Albany NY)* **12**, 20471–20482 (2020).
27. S. Y. Hsieh *et al.*, Comparative proteomic studies on the pathogenesis of human ulcerative colitis. *Proteomics* **6**, 5322–5331 (2006).
28. I. Okayasu *et al.*, A novel method in the induction of reliable experimental acute and chronic ulcerative colitis in mice. *Gastroenterology* **98**, 694–702 (1990).
29. C. Hidalgo-Cantabrana *et al.*, Effect of a ropy exopolysaccharide-producing Bifidobacterium animalis subsp. lactis strain orally administered on DSS-induced colitis mice model. *Front. Microbiol.* **7**, 868 (2016).
30. B. B. Madison *et al.*, Cis elements of the villin gene control expression in restricted domains of the vertical (crypt) and horizontal (duodenum, cecum) axes of the intestine. *J. Biol. Chem.* **277**, 33275–33283 (2002).
31. L. A. O'Neill, R. J. Kishton, J. Rathmell, A guide to immunometabolism for immunologists. *Nat. Rev. Immunol.* **16**, 553–565 (2016).
32. D. R. Donohoe *et al.*, The microbiome and butyrate regulate energy metabolism and autophagy in the mammalian colon. *Cell Metab.* **13**, 517–526 (2011).
33. D. J. Kominsky, E. L. Campbell, S. P. Colgan, Metabolic shifts in immunity and inflammation. *J. Immunol.* **184**, 4062–4068 (2010).
34. A. Subramanian *et al.*, Gene set enrichment analysis: A knowledge-based approach for interpreting genome-wide expression profiles. *Proc. Natl. Acad. Sci. U.S.A.* **102**, 15545–15550 (2005).
35. C. Becker, M. F. Neurath, S. Wirtz, The intestinal microbiota in inflammatory bowel disease. *ILAR J.* **56**, 192–204 (2015).
36. C. Michaudel, H. Sokol, The gut microbiota at the service of immunometabolism. *Cell Metab.* **32**, 514–523 (2020).
37. K. L. Glassner, B. P. Abraham, E. M. M. Quigley, The microbiome and inflammatory bowel disease. *J. Allergy Clin. Immunol.* **145**, 16–27 (2020).
38. I. Khan *et al.*, Alteration of gut microbiota in inflammatory bowel disease (IBD): Cause or consequence? IBD treatment targeting the gut microbiome. *Pathogens* **8**, 126 (2019).
39. K. Matsuoka, T. Kanai, The gut microbiota and inflammatory bowel disease. *Semin. Immunopathol.* **37**, 47–55 (2015).
40. S. Stojanov, A. Berlec, B. Strukelj, The influence of probiotics on the Firmicutes/Bacteroidetes ratio in the treatment of obesity and inflammatory bowel disease. *Microorganisms* **8**, 1715 (2020).
41. C. J. Sui *et al.*, MicroRNA-147 suppresses human hepatocellular carcinoma proliferation migration and chemosensitivity by inhibiting HOXC6. *Am. J. Cancer Res.* **6**, 2787–2798 (2016).
42. L. Li *et al.*, A solute carrier family 22 member 3 variant rs3088442 G->A associated with coronary heart disease inhibits lipopolysaccharide-induced inflammatory response. *J. Biol. Chem.* **290**, 5328–5340 (2015).
43. Z. Wu *et al.*, OMA1 reprograms metabolism under hypoxia to promote colorectal cancer development. *EMBO Rep.* **22**, e50827 (2021).
44. K. Pollecker, M. Sylvester, W. Voos, Proteomic analysis demonstrates the role of the quality control protease LONP1 in mitochondrial protein aggregation. *J. Biol. Chem.* **297**, 101134 (2021).
45. Y. Han *et al.*, A human iPSC-array-based GWAS identifies a virus susceptibility locus in the NDUFA4 gene and functional variants. *Cell Stem Cell* **29**, 1475–1490.e6 (2022).
46. C. Garrido *et al.*, Mechanisms of cytochrome c release from mitochondria. *Cell Death Differ.* **13**, 1423–1433 (2006).
47. X. Guo *et al.*, Mitochondrial stress is relayed to the cytosol by an OMA1-DELE1-HRI pathway. *Nature* **579**, 427–432 (2020).
48. X. Ning, C. Wang, M. Zhang, K. Wang, Ectopic expression of miR-147 inhibits stem cell marker and epithelial-mesenchymal transition (EMT)-related protein expression in colon cancer cells. *Oncol. Res.* **27**, 399–406 (2019).
49. D. K. Chan, C. L. Leggett, K. K. Wang, Diagnosing gastrointestinal illnesses using fecal headspace volatile organic compounds. *World J. Gastroenterol.* **22**, 1639–1649 (2016).
50. C. E. Garner *et al.*, Volatile organic compounds from feces and their potential for diagnosis of gastrointestinal disease. *FASEB J.* **21**, 1675–1688 (2007).
51. M. Boldin, Effect of depletion of *C15ORF48/miR-147* on gene expression in primary colonocytes. https://www.ncbi.nlm.nih.gov/geo/. Deposited 23 October 2023.